How Physics can help in understanding Cardiac Rhythms ?

Predicting & Control of complex oscillatory behavior

Shiuan-Ni Liang[1], Duy Manh Le[2,3], Wei-Yin Chiang[4], Pik-Yin Lai[1*], and C. K. Chan[1,2]
[1]Dept. of Physics and Center for Complex Systems, National Central University, Chung-Li, Taiwan 320
[2]Institute of Physics, Academia Sinica, Nankang, Taipei 115, Taiwan
[3] Institute of Physics, VAST, 10 Dao Tan, Ba Dinh, Hanoi, Vietnam
[4]Dept. of Physics, Harvard University, 17 Oxford Street, Cambridge, MA 02138, U.S.A.

*e-mail: pylai@phy.ncu.edu.tw

Abstract— **We discuss our recent theoretical and experimental work in cardiac systems. The first is about the rhythmic variation as the cardiac myocyte cell culture synchronized, and how it can be explained in terms of the frequency enhancement phenomenon in coupled excitable systems. Another work concerns the prediction of self-terminating ventricular fibrillations (VF) based on the analysis of time-series signals from ventricles and near the sinus atrial node by the cross-wavelet power spectrum and cross-Fourier power spectrum methods. The success rate of our prediction criteria is about 80-90%. Our findings suggest that a heart under VF can recover its sinus rhythm only when the sino-atrial node of the heart is not under strong influence of the VF from its ventricle. Finally the dramatic reduction of cardiac alternans by small perturbations in pacing scheme. Alternans are alternating long and short action potential durations in heart beats, which is a precursor of the fatal. Predictions and validity of this control method have been verified by both experiments performed with isolated heart preparations and numerical simulations. A nonlinear return map for this novel pacing scheme based on action potential duration restitution response is proposed to explain the working mechanism of the control. Extending this novel control method to general complex dynamics can be achieved.**

Keywords – cardiac rhythm, frequency enhancement, ventricular fibrillations, cardiac alternans, nonlinear dynamics, time-series analysis

I. INTRODUCTION

Biological rhythms often show a certain degree of variations under different conditions. A well-known example is synchronization of insects such as the blinking of fireflies or chirping of crickets. It had been observed that the frequency of chirps from snowy tree crickets change in order to synchronize with their neighbors. In neuroscience, changes in neuron spike frequency arising during immobilization catatonia continued after the animals recovered from this state. Since most of these neurons have similar structures and ion-channels, the variations in their resultant temporal activities are presumably due to the coupling effects among the neurons. From a biological point of view, it would be advantageous if the cells can adjust their spiking frequency by changing the coupling strength instead of varying their intrinsic time scales. An example is the heart beating rate variations. The mean and variance of beat intervals of rat can be varied under different temperatures. Also, the frequency of heart beat in vivo is about seventy times per minute for human while it is about two hundred times per minute for rats. For an individual cell, no matter for rat or human, the activation mechanism due to the ion-channels that lead to oscillation is similar. By different cell-cell interactions/connections, the emergent dynamical behavior can vary in a wide range. From the medical point of view, the maintenance of normal heart beat is vital for keeping an organism health is often regulated by the nervous, respiratory and circulation systems. And the question of avoiding cardiac arrhythmia and understanding their mechanism, both physiological and dynamical, are of practical and fundamental importance. A cardiac system, no matter it is composed of cardiac myocytes incubated in culture, an intact cardiac tissue, or a whole heart in vitro or in vivo, is a periodic beating system and can be investigated in terms of nonlinear dynamics, such as nonlinear oscillators. In this paper, we review our recent research on topics related to cardiac oscillatory systems, with emphasis on how nonlinear physics can helps us to understand the basic mechanism in several cardiac arrhythmia phenomena, and the collective cardiac rhythm resulted due to the coupling of individual entities. With a thorough understanding of the physics behind these complex phenomena, feedback control can be devised to manipulate and control the cardiac dynamics in some situations.

II. FREQUENCY VARIATION AND SYNCHRONIZED BEATING IN CULTURED CARDIAC CELLS

Experiments designed to study the synchronization process of a self-assembled heterogenous system using dissociated cardiac cultures are carried out. Details of the experiments can be found in [1]. Briefly, cardiac cells are obtained from the ventricles of postnatal (2-3 days) mice. Tissues of the ventricles from about 10 mice are dissociated and re-suspended as cell suspensions. There are two major types of cells in the cell suspensions; namely cardiac myocytes (CM) and fibroblasts. Fibroblast in the cell suspensions are further removed by incubating the cell suspensions in a flat bottle flask at 37^{o}C for two hours. Cells re-suspended from these flasks after this procedure usually

contain about 10 to 20% fibroblast. In the preparation of our samples, we control the initial plating density of the cells to be around 10^6 cells/cm^2. Cells are plated on 9.6 cm^2 Petri dishes with no coating for further observations on a microscope equipped with an incubator (37°C and 5% CO_2). Optical images from the microscope are digitized and processed by a computer.

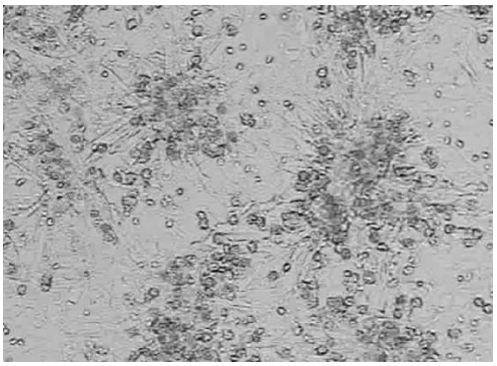

Figure 1. Morphologies of the cardiac cell culture under bright field microscopy showing cells cluster together forming synchronized beating.

Fig. 1 shows the morphology of the cultures under bright field microscope. Immediately after plating (t = 0), the CM are well dispersed and there are no beatings of the cells. Once the cells are plated, there are aggregations of the CM to form clusters. Note that the empty spaces left behind during the aggregation are not really empty. They will be occupied by fibroblasts after their proliferations. Beatings of the CM in the clusters can be observed at about t = 5 hours and will be synchronized as the clusters grow. However, the growth of the cluster will stop at about t = 20 ~ 24 hours when the size of the cluster is about 70 microns. Synchronization among these clusters increases gradually afterward and total synchronized beating among the clusters can be observed at about t = 40 hours. The beating of the clusters are monitored by an image analysis program which detects motions of the clusters in video images similar to those shown in Fig. 1. A video image is divided into 16 x 16 squares and the beatings of these 256 squares are recorded at 24 frames/sec for three days. The time dependence of the beatings of these 256 squares will provide 256 channels of data. To quantify the degree of synchronization among these 256 channels, the method of principle component analysis is used.

There is a significant variation in heart beating rates in the culture medium formed by fibroblast and cardiac myocytes and the beating eventually become synchronized. As the beating of the cells is approaching synchronization, there is a maximum mean beating rate as the culture develops. The mean beating frequency increased with time, has a maximum (from 1.4 to ~2.3 Hz, enhanced by ~ 65%), and then synchronized (see Fig. 2a). The synchronized frequency is enhanced by ~ 35% (from 1.4 to ~1.9 Hz).

The experimentally observed beating rate variation can be understood qualitatively in terms of the frequency enhancement phenomenon in our model of coupled excitable elements [2]. To further mimic the cardiac cell culture experiments and aim at modeling the system more quantitatively, we perform simulation of coupled excitable FitzHugh-Nagumo (FHN) elements on a two-dimensional square lattice. In the FHN model, the resting state and excited states correspond to phase 4 and phase 2 in cardiac action potential, respectively.

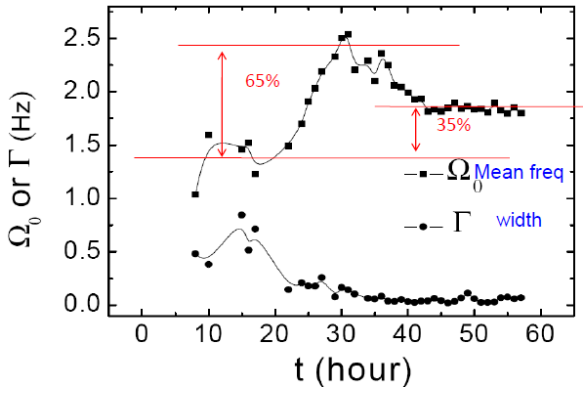

(a)

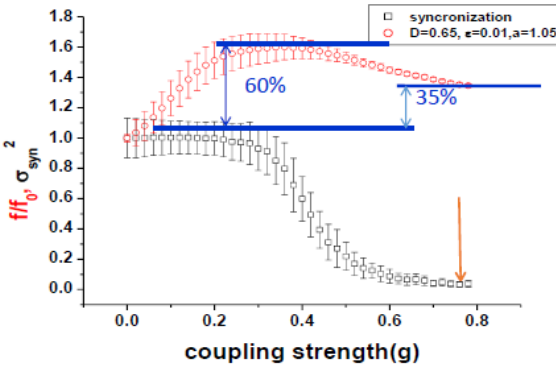

(b)

Figure 2. (a) Measured time dependence of the mean frequency and the width of the distribution of the beatings of the clusters during the synchronization process. Note that the mean frequency can increase up to a maximal of about 65% before it settled down to about 35% increase as the system synchronized. Solid lines are used only to guide to the eyes. (b) Simulation results of coupled noisy excitbale FitzHugh-Nagumo elements (on a 55x55 square). The mean frequency shows about a 60% of frequency enhancement before it settles down to about a 35% increase as the system synchronized at large coupling (indicated by the brown arrow).

Each FHN element is identical and coupled to its nearest neighbors with the same coupling g, but each element is subjected to independent uncorrelated noises. Simulation is carried out on a square lattice and the beating frequency distribution of these elements are recorded for different values of coupling strengths g. Fig. 2b shows the mean beating frequency together with the width of the frequency distribution as a function of g. The width of the frequency distribution also characterizes the degree of synchronization.

The beating rate initially increases with low values of coupling strengths, attains a maximum as the cells become synchronized. There is a peak enhancement of about 60% and an enhancement of about 35% when the system almost fully synchronized, which agrees quantitatively well with the experimental data.

III. Predicting Self-terminating Ventricular Fibrillation

Ventricular fibrillation (VF) is a fatal cardiac arrhythmia in which the heart cannot contract in a coordinated manner and hence blood cannot be pumped properly. However, under some rare situations, VF can stop by itself without any external intervention, a well-documented clinical phenomenon known as self-terminating VF (STVF).

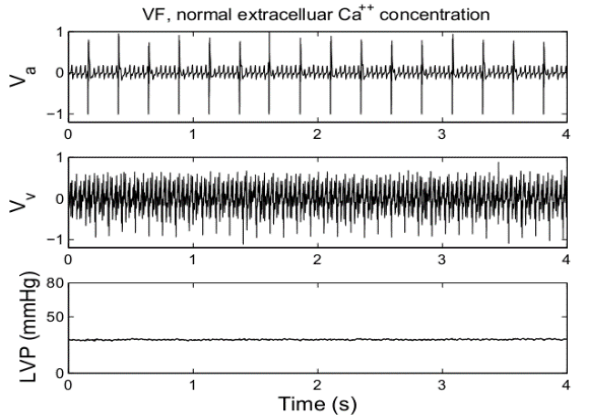

(a)

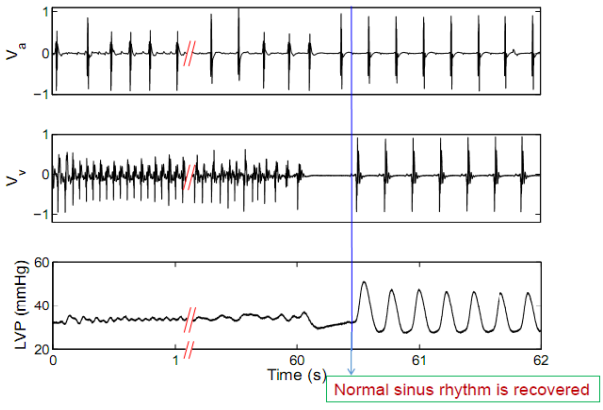

(b)

Figure 3. Time-series measurements of the right atrium (V_a), ventricle (V_v) potentials, and left-ventricle pressure (LVP). Left: for the case of sustained ventricular fibrillation. Right: self-terminating ventricular fibrillation The blue arrow indicates the time normal sinus rhythm is recovered.

A question of both fundamental and practical interest STVF would be: are there any signs from the measured heart beat signals which can be used to distinguish between cases of STVF and non-STVF? The answer to this question would shed light to the understanding of the mechanism in STVF. For this issue, we designed isolated heart experiments to answer this question [3]. In our experiments, electrical signals measured at two locations, one on the right atrium very close to the SA node (V_a) and the other from the ventricle (V_v), of a heart under VF are analyzed to search for the sign to distinguish between STVF and non-STVF. Fig. 3 shows typical V_a and V_v signals during VF and STVF, along with the left ventricle pressure (LVP) measurements. It is reasonable to assume that there are hidden relations between atrium and ventricle signals due to the coordinated beatings of the normal functioning heart. From the bivariate time series data (ECGs), two data analysis methods, namely Cross Wavelet Spectrum (XWS) and Cross Fourier Spectrum (XFS), are employed to figure out the precursor characteristics for the cases in which VFs can self-recover or not.

Cardiac arrhythmic dynamics were carried out in an isolated whole heart using the Langendorff system, shown schematically in Fig. 4. Briefly, the Langendorff system is used to maintain the physiological condition of an isolated heart and keep it alive by providing perfusion with nutrient rich, oxygenated solution at a constant temperature. In our experiments the hearts were extracted from Wistar rats (weight between 250g to 300g, both males and females). Usually, the preparation can last for three to four hours. In the experiment, pseudo-ECGs of the hearts at various parts are monitored by inserting the electrodes in the heart tissues.

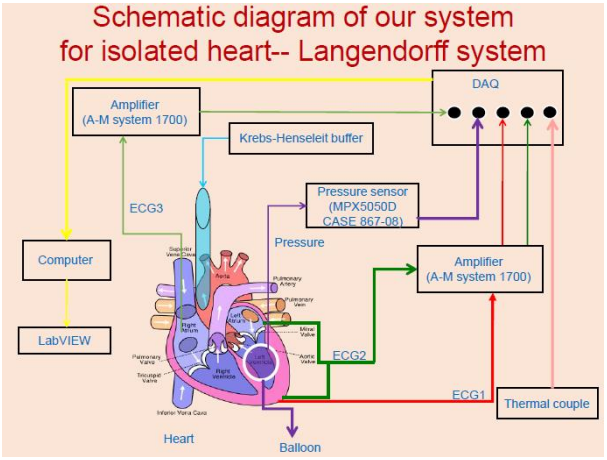

Figure 4. Schematic picture showing the isolated whole heart experiment. A small water-filled balloon is placed inside the left ventricle to measure the cardiac contraction pressure.

A pacing electrode placed on the septum between two ventricles is used to provide controlled stimulation to the isolated heart. The contraction pressure of the left ventricle

(LVP) is monitored by a water-filled latex balloon inserted inside the left ventricle through a pressure transducer.

A. *Cross Fourier Spectrum Analysis*

Denoting the discrete Fourier components of the time-series X by X_k. The Fourier Power Spectrum (FPS) of time-series X and Cross Fourier Spectrum (XFS) of two time-series (X and Y) are defined respectively as FPS=$|X_k|$ and XFS=$|X_k\ Y_k^*|$. Fig. 5 shows the typical Fourier spectra of V_a, V_v and their XFS for both the STVF and non-STVF cases. It is clear that the V_a of STVFs have a widely distributed FPS as shown in the bottom panel. Since the power is distributed over a broad frequency range its amplitude is small. Notice that the FPS of V_v is usually localized at some frequency (middle panel) close to the frequency of fibrillation. This leads to the small dominant power in the XFS (top panel). In contrary to the STVFs, FPS of V_a from the non-STVF episodes are characterized by higher powers at some harmonics of RA rhythm for the case that its own beating is quite regular and highly nonlinear (bottom panel), and the power of the FPS of V_v is highly localized at the frequency of fibrillation (middle panel). As a result, the dominant power in the XFS of non-STVF episodes becomes very high in comparison to the case of STVF.

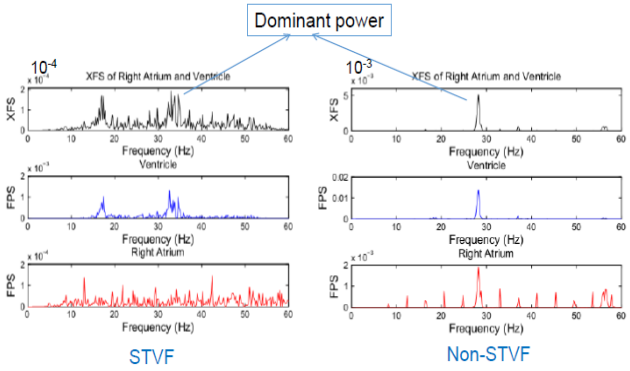

Figure 5. Fourier spectrum analysis of STVF and non-STVF episodes. Left: A typical STVF episode. The top, middle, and bottom panels corresponding to the XFS of RA and ventricle signals, the FPS of ventricle, and FPS of RA respectively. In this episode, the dominant frequency of ventricle is about 32 Hz which is the same as the dominant frequency of the XFS, whereas the FPS of the RA signal is spread over a wide range of frequencies. Right: A typical non-STVF. The dominant frequencies of both ventricle and RA signals are about 28 Hz, resulting in the same dominant frequency of the XFS with a high dominant power.

Fig. 6 is a summary of the values of the dominant power of XFS between V_a and V_v for all the VF episodes. The group of STVFs is shown in gray and the non-STVF group is shown in black. This chart suggests that VF with a high dominant power has little chance for STVF, whereas the VF with a low dominant power has a very good chance to recover to its normal rhythm. It can be seen easily in Fig. 6 that there are two well separated groups: group 1 with low dominant power (say lower than 0.004) on the left that contains 28 episodes out of which 25 are STVF. Thus one can say that the VF sample with a low dominant power has high chance (~89%) to survive. Group 2 with high dominant power (higher than 0.004) contains 10 episodes and all of them are non-STVF (100%). When the dominant power of XFS is high, VF has little or no chance to self-terminate.

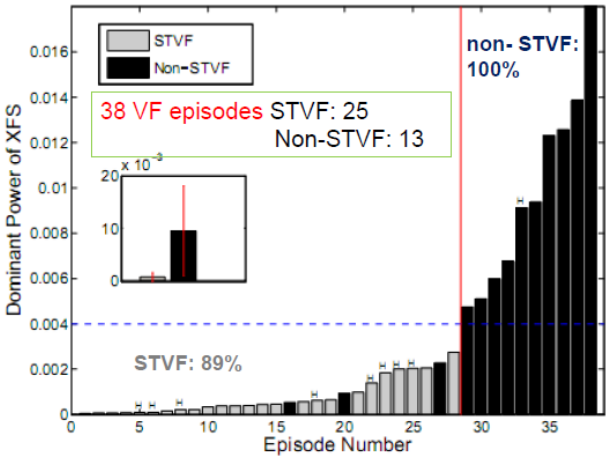

Figure 6. Signatures of STVF and non-STVF episodes for all 38 samples from 11 hearts. 25 STVF and 13 non-STVF scenarios, as revealed by the XFS method. The dominant power of XFS of right atrium and ventricle signals. The inset shows the average dominant XFS of the non-STVFs is much larger than that of the STVFs.

B. *Cross Wavelet Spectrum Analysis*

For a further independent analysis of the same data, we employed the Cross Wavelet Spectrum (XWS) to figure out the signatures for the STVF and non-STVF cases. The wavelet of a time series x_n is defined as

$$W_n^X(s) = \sqrt{\frac{\delta t}{s}} \sum_{n'=0}^{N-1} x_{n'} \Psi_0[(n-n')\frac{\delta t}{s}], \quad \Psi_0(\eta) = \pi^{-\frac{1}{4}} e^{i\omega_0\eta} e^{\frac{1}{2}\eta^2}$$

where Ψ_0 is the mother wavelet function with Morlet wavelet of ω_0=6. And the XWS between two time series is defined as $|W^X W^{Y*}|$. The precursors of STVF and non-STVF can be characterized by the XWS and the distribution of these powers over different frequencies. Fig. 7 displays the time traces and the corresponding XWS between signals from V_a and V_v for both the STVF and non-STVF cases. The area of 5% significant power in the XWS is employed to indicate regions of strong power. The total area (A) enclosed by the top 5% power contours near the fibrillation frequencies provides a measure of the strength or significance of the wavelet spectrum. The distribution of these strength in frequency can be measured by the standard deviation, σ, of the P(f) which is the time average of the XWS. A small σ indicates that these powers are concentrated in a small frequency range and vice versa.

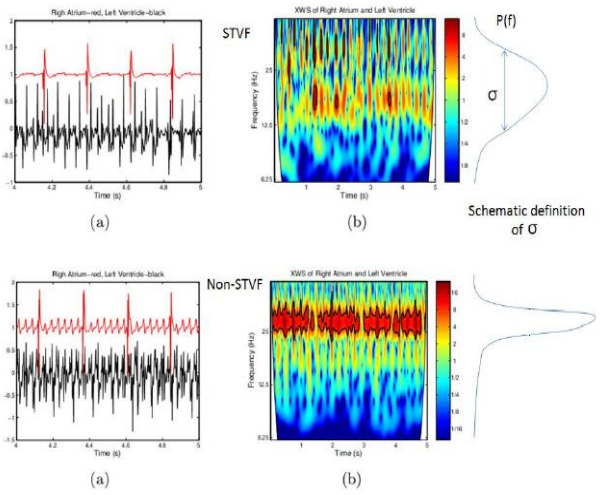

Figure 7. Wavelet spectrum analysis of a typical STVF (upper panel) and non-STVF (lower panel) episodes. (a) the time series (of 1 second duration) of RA (red upper trace) and ventricle (black lower trace) signals. (b) Time-frequency plot showing the color coded power of the XWS of the RA and ventricle signals. In each time-frequency plot, significance tests are carried out on the wavelet spectra to remove spurious power. The thick contour shows the 5% significant level against noise. The frequecy distribution P(f) and its width , σ, are also shown schematically.

Fig. 8 is the results of using A and σ to characterize the influence of V_v on V_a for all the 38 VF episodes in our experiments. It can be seen from the Fig. 8 that most of non-STVFs fall into a region with A > 0.9 and σ <10 and most of STVFs are outside this region. We find that 23 out of the 25 STVF episodes have either small A or large A together with a large σ as depicted in Fig. 3. Also, 9 out of the 13 non-STVF episodes are characterized by large A and small σ.

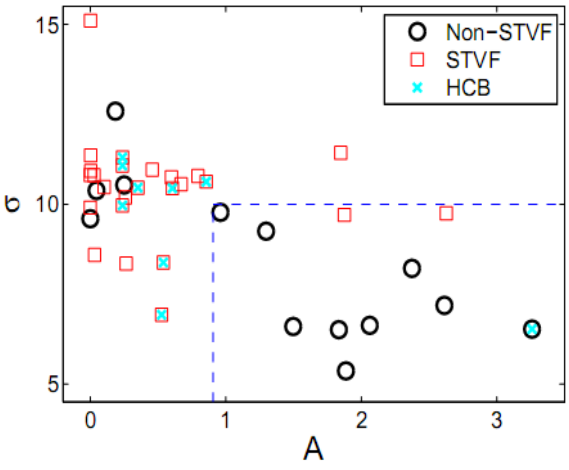

Figure 8. Signatures of STVF and non-STVF episodes for the same 38 samples as revealed by the XWS method. Standard deviation, σ, of P(f) vs. the total area A enclosed by 5% significance level contours near the fibrillation frequencies.

Therefore, if the criteria of large A and small σ is used (the region bounded by the dashed lines in Fig. 3) for predicting non-STVF, the successful rate is about 82%. On the other hand, with the criterion of A is small or A is large but with large σ (outside the dashed rectangle) to predict the occurrence of STVF, the successful rate is about 85%.

IV. Dramatic Cardiac Alternans Reduction by Feedback Control

Cardiac alternans [4] are alternating long and short durations of action potential durations (APD), which also manifested in alternating strong and weak cardiac contractions or pulses. Fig. 9 illustrates schematically the time-series of APD during alternans under periodic external pacing (indicated by arrows). Alternating short and long APDs occur when the external pacing is sufficiently rapid.

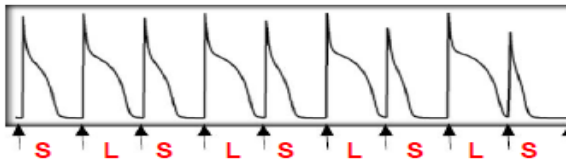

Figure 9. Schematic figure showing the development of APD alternans under periodic external pacing (indicated by black arrows). Alternate short and long APDs are indicated by S and L respectively.

It is known that alternans are generated because of the nonlinear recovery property of the heart. Usually, this nonlinear property of the heart is expressed as a restitution curve *f*, relating the APD of the nth beat (denoted by A_n) to the previous diastolic interval (DI): $A_n = f(DI_{n-1}) = f(T - A_n)$, where *n* is the beat number. For slow pacing (large *T*), $A^* = f(T - A^*)$ is a stable fixed point and there is no alternans. But for sufficiently fast pacing (small *T*), the fixed point becomes unstable and gives rise to alternans. Instead of measuring directly the APD, we monitored the LVP which has a one-to-one correspondence to the cardiac contraction and hence the APD. Again, isolated whole heart experiments were setup with cardiac alternans induced by rapid pacing. Here we briefly outline the idea of our recently proposed *T*+*T*- feedback control method [5] for dramatic reduction of alternans magnitude by small perturbations. Conceptually, the *T*+*T*- control scheme simply alters the pacing cycle length by a fixed small amount ε according to the rule:

$$T_n \rightarrow T + \varepsilon \quad \text{if} \quad A_n > A_{n-1}$$
$$T_n \rightarrow T - \varepsilon \quad \text{if} \quad A_n < A_{n-1}.$$

To examine the detail mechanism of our control scheme, we carried out simulation of the Luo-Rudy I model (LR1) [6] in which the membrane potential *V(t)* is governed by

$$C_m \frac{dV}{dt} = -I_{ion}(V, g_i) + I_{stim}(t)$$

where C_m is the transmembrane capacitance, I_{stim} is the stimulus current, I_{ion} is the total current density through various ion channels on the cellular membrane, and g_i describe the dynamics of gating conductance of different ion channels. LR1 is one of the simplest ion-channel model for cardiac cell that takes into account the basic currents for a

cardiac cell to perform the action potential, whose total current density is composed of six essential currents:

$$I_{ion} = I_{Na} + I_K + I_{Ca} + I_{Kp} + I_{K_1} + I_b$$

I_{ion}, consists six ionic currents: a fast inward sodium current I_{Na}, which is primarily responsible for the rapid upstroke of the action potential; a slow inward current I_{Ca} that mainly carries calcium ions and plays a dominant part in the creation of the myocardial APD plateau; a time-dependent potassium current I_K, which repolarizes the membrane to rest; a time-independent inward-rectifying potassium current I_{K1} responsible for stabilizing the resting membrane potential; a plateau potassium current I_{Kp} activating only at plateau potential; and a background potassium current I_b that exists at negative potentials after blocking I_{K1}. External pacing and feedback control is carried out by $I_{stim}(t)$.

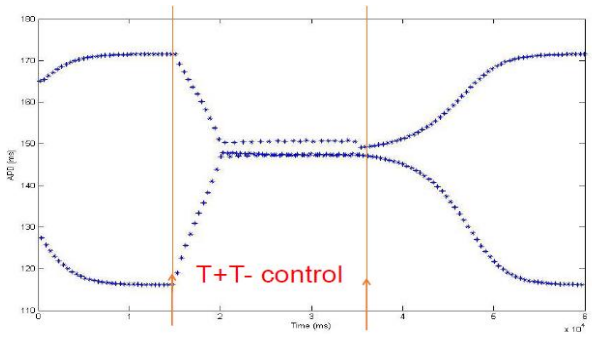

(a)

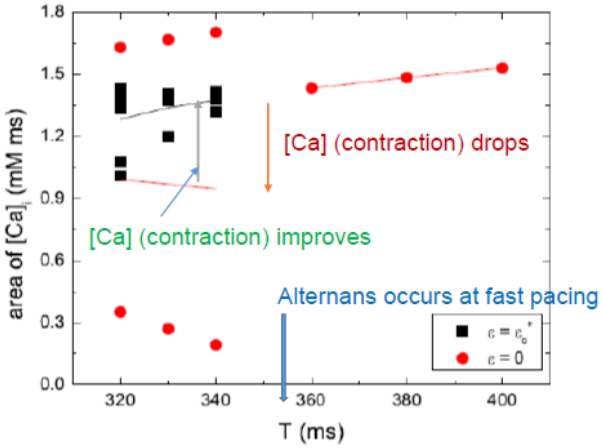

(b)

Figure 10. Simulation results of *T+T-* feedback control of alternans using the Luo-Rudy I model. (a) APD time-series with the control being applied from t=15 to 35s as indicated by the arrows. (b) Area of time variation of $[Ca]_i$ curve in a beat for no control ($\varepsilon = 0$, red filled circle) and when the control is turned on with just above the critical value (black square) at different base pacing period T for $g_K = 0.282$. Solid and dashed curves represent the time averages.

In our isolated whole heart experiments [5], it is more convenient to perform the control on the ventricle pressure of the heart. In fact, it is the contraction strength or ventricle pressure that has the direct physiological effects on the patient. Thus for the simulation using the LR1 model, instead of detecting the APD for feedback, the peak intracellular Ca concentration $[Ca]_i$ is used as the control signal. Fig. 10a shows the time-series of APD measured from the simulation results with *T+T-* control being applied from t=15s to 35s, showing the alternans is greatly suppressed during the control. Furthermore, Fig. 10b shows that the average areas of $[Ca]_i$ during the control are larger compared to the case when the alternans are not controlled. This implies that the average strength of the cardiac contraction is improved under our *T+T-* scheme.

This unconventional control scheme has been tested by an isolated whole heart preparation. The experimental setup is similar to that described in Fig. 4. *T+T-* control scheme is implemented using the peak LVP as the feedback signal since it is known that there is a one to one correspondence between LPV and APD. Therefore, in our experimental implementation, T_n depends on the sign of $P_n - P_{n-1}$ where P_n is the peak value of nth peak in the measured LVP. Fig.11 shows the time course of P_n in a typical control experiment. Notice that the alternans magnitude is reduced to a negligible level after the control is turned on.

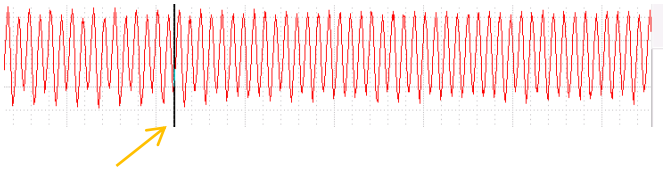

Figure 11. Experimental *T+T-* feedback control of an isolated heart in alternans state. Time series data of the LVP. The arrow indicates the time at which the control is applied. After some time the magnitude of the alternans is greatly reduced.

V. Final Remarks and Outlook

Here we would like to point out the traditional approach for controlling dynamical systems has been stabilizing unstable orbits, and much research has been devoted to use feedback control to avoid chaotic dynamics by stabilizing the otherwise unstable periodic orbits [8]. However, in *T+T-* control, the mechanism for the success of the control is by introducing small chaotic attractor to trap the system dynamics. Thus, we do not control chaos, instead chaotic dynamics is generated by our feedback control and stays there. The unstable periodic (period-1) orbit is never stabilized by our control. Under a successful control, the originally stable period-2 orbit gives way and the system is trapped in the localized chaotic attractor generated by the control. On the other hand, our recent thorough theoretical investigation [9] for the nature of this alternans reduction revealed the basic mechanism behind the control in terms of

the new idea of confining the dynamics using localized chaotic attractors. Using the cardiac restitution model, analytic results can be obtained, such as the existence of the critical ε_c and how it can be calculated analytically, as well as the coexistence of the stable alternans fixed points and the chaotic attractor for $\varepsilon < \varepsilon_c$ and hence leads to the possibility of alternans suppression even for $\varepsilon < \varepsilon_c$. In addition, the nature of the chaotic attractor dynamics with specific transitions is revealed and can remarkably be observed in the refined experiments [9].

Such a novel idea of using localized chaotic attractor to control/confine the dynamics of a system is rather general and can be applied to other systems, thus we believe it will have a broad impact on other physical systems. It can be shown that the *T*+*T*- control method can be extended to control complex periodic motion to low periodic states and even taming chaotic motion to the desired periodic motion. We have recently implemented such a control scheme on the chaotic compass under an oscillating magnetic field, and successfully control the motion otherwise complex or chaotic dynamics to the desired ordered motion.

ACKNOWLEDGMENT

These works have been supported by the Ministry of Science and Technology of Taiwan and National Center for Theoretical Sciences of Taiwan.

REFERENCES

[1] W. Chen, S. C. Cheng, E. Avalos, O. Drugova, G. Osipov, P. Y. Lai, and C. K. Chan, "Synchronization in growing heterogeneous media ", Europhys. Lett. **86**, 18001(2009).

[2] W. Y. Chiang, P. Y. Lai, and C. K. Chan, "Frequency Enhancement in Coupled Noisy Excitable Elements", Phys. Rev. Lett. **106**, 254102 (2011). "Frequency Enhancement in coupled noisy excitable elements: Effects of network topology", Eur. J. Phys. B **86**, 327 (2013).

[3] D. M. Le, A. V. Dvornikov, Pik-Yin Lai, and C. K. Chan, "Predicting Self-terminating Ventricular Fibrillation in an Isolated Heart", Europhys. Lett. **104**, 48002 (2013). (Editor's choice)

[4] A. Karma and R. F. Gilmour, "Nonlinear dynamics of heart rhythm disorders", Phys. Today March, 51 (2007).

[5] S. Sridhar, D.-M. Le, Y. C. Mi, S. Sinha, P. Y. Lai, and C. K. Chan, "Suppression of cardiac alternans by alternating period feedback stimulations", Phys. Rev. E **87**, 042712 (2013).

[6] C. H. Luo and Y. Rudy, "A model of the ventricular cardiac action potential. Depolarization, repolarization, and their interactions", Circ. Res. **68**, 1501 (1991).

[7] S. N. Liang, D.M. Le, Pik-Yin Lai, and C. K. Chan, "Ionic characteristics in Cardiac alternans suppression using T+/- feedback control ", preprint.

[8] "Handbook of Chaos Control, 2nd ed.", E. Schöll and H. G. Georg Schuster (editors), (Wiley 2008).

[9] D. M. Le, Y. T. Lin, Y. H. Yang, P. Y. Lai, and C. K. Chan, "Suppression of Cardiac Alternans by Chaotic Attractors", preprint.